Scientific Research Publishing

Journal of Materials Science and Chemical Engineering, 2025, 13(9), 96-114
https://www.scirp.org/journal/msce
ISSN Online: 2327-6053
ISSN Print: 2327-6045

Investigation of the Solution-Dependent Zinc Oxide (ZnO) Thin Film Growth Process by the Electrostatic Spray Deposition (ESD) Method

Fysol Ibna Abbas[1,2,3*], Mutsumi Sugiyama[2,3,4]

[1]Department of Electrical & Electronics Engineering, Faculty of Science & Technology, City University, Dhaka, Bangladesh
[2]Department of Electrical Engineering, Tokyo University of Science, Tokyo, Japan
[3]Poster Presenter, 2025 E-MRS Spring Meeting, Convention & Exhibition Centre of Strasbourg, Strasbourg, France
[4]National Research Institute, RIST, Tokyo University of Science, Tokyo, Japan
Email: *fysolibnaabbas1988@gmail.com

How to cite this paper: Abbas, F.I. and Sugiyama, M. (2025) Investigation of the Solution-Dependent Zinc Oxide (ZnO) Thin Film Growth Process by the Electrostatic Spray Deposition (ESD) Method. *Journal of Materials Science and Chemical Engineering*, **13**, 96-114.
https://doi.org/10.4236/msce.2025.139007

Received: August 15, 2025
Accepted: September 19, 2025
Published: September 22, 2025

Abstract

The present study describes a facile route of nanocrystalline (NC) ZnO growth using the solution-dependent ESD method at temperatures ranging from 300˚C to 500˚C. Zinc chloride ($ZnCl_2$) was used as the Zn source, and it was dissolved in ethanol (CH_3CH_2OH) to prepare the various ESD spray solutions. The crystallographic orientations of the ZnO thin films were evaluated using X-ray diffraction (XRD). The morphologies of the ZnO films were observed by scanning electron microscopy (SEM). In order to check for the material composition of ZnO films, the energy-dispersive X-ray spectroscopy (EDX) analysis was performed. XRD and Raman show that ZnO thin films have a hexagonal wurtzite structure and point out a possible complex reaction mechanism due to the increase in H_2O ratio in the solution. The microstructural parameters (MIP), namely, lattice parameters, were revealed using Bragg's law. Meanwhile, other MIPs, such as bond length, positional parameters of the lattice phase, full width at half maximum, crystallite sizes, lattice strain, and lattice dislocation density, were estimated using the Debye-Scherrer method (D-S). The findings indicate that the ratio of added deionized water (H_2O) suppresses the c-axis crystal growth of ZnO thin films. The adhesion of anions is thought to be responsible for this suppression. The results and analysis gave clues about how to develop a high-quality oxide-based crystal semiconductor that is economically viable for industrial and commercial applications of the ESD technique to semiconductor technology devices.

Keywords

Electrostatic Spray Deposition, Debye-Scherrer Analysis, ZnO Thin Film

1. Introduction

ZnO nanostructures have been the focus of significant research because their potential for use as a material in various fields, including solar cells [1], light-emitting diodes [2] [3], photocatalysis [4], gas sensors [5], catalysis [6], laser diodes [7], varistors [8] and sensors [9], is promising. ZnO is a widely recognized *n*-type semiconductor with a wide band gap of approximately 3.37 eV and a substantial exciton binding energy of around 60 meV at ambient temperature [10]. However, the use of the methodologies for ZnO nanostructures is restricted due to factors such as elevated temperature, precise gas concentration, hazardous chemical reagents, and expensive equipment. Various deposition methods, including wet and dry processes, are employed to create ZnO thin films, such as sputtering [11], pulsed laser deposition [12], chemical bath deposition [13], mist chemical vapor deposition [14], spray processes [15] [16], and the sol-gel method [17] [18]. Among these, the spray process is highlighted by its cost-effectiveness and simplicity, as it operates under air conditions, making it suitable for manufacturing on a large scale, utilizing roll-to-roll fabrication methods.

In this study, the current goal is to create a simple and cost-efficient method that can be easily expanded for commercial use for thin film fabrication. ESD is a highly attractive technique, particularly in spray applications, owing to its capability to generate submicron-sized droplets and manipulate their movement using an external electric field source [19]-[26], as shown in **Figure 1(a)**. Under the present circumstances, ESD application on thin film fabrication aims fourfold, not only to study the ZnO thin film growth mechanism but also to investigate different crucial MIP analyses of the nanocrystal particle sizes for the development of high-quality crystal growth for oxide-based semiconductor technology. Firstly, the literature review results indicate that the growth mechanism of ZnO thin films using the ESD technique has not been documented within this specific combination of samples and temperature ranges. Secondly, the ESD approach offers user-friendly functionality with significant industrial advantages, including its capacity to effectively cover extensive regions due to its uncomplicated and easily accessible nature. Thirdly, the ESD method enables deposition without requiring a vacuum, is reasonable, and offers relatively easy control of the composition ratio and doping. Fourthly, within the ESD application for thin film fabrication, the functionality of "cone-jet mode" was tried to be revealed for the optimum correlation of the thin film growth mechanism. Both theory and experimental processes in literature [27]-[29] reveal that by adjusting the applied voltage, one can also control the flow rate. Moreover, by applying a high voltage, a stable flow rate can also be obtained; as a result, the spray area can also be generated in a large possible region. The current study tests this phenomenon to fabricate thin films on a large area of the substrate surface. The working principle for this "cone-jet mode" is electrostatic atomization for liquids of relatively high conductivity; the conical form of the meniscus results from a static equilibrium between capillary, hydrostatic, and electrostatic pressures. Furthermore, when conductivity is low, this ac-

celeration zone can begin at the outlet of the capillary, and the conical form is more or less marked depending on the flow rate of the fluid, the size of the capillary, and the applied voltage. In addition, the appropriate high voltage and the corresponding flow rate are mentioned in Table 1 as the ESD parameter.

Furthermore, from the physics perspective, Coulomb forces caused charged droplets to repel each other, preventing them from colliding during the spray on the ITIO substrates. These features allow for the creation of dense and homogeneous thin films using ESD to cover the large area on the surface of the ITIO substrates. The crystal quality of ZnO thin films deposited through ESD was evaluated to determine the suitability of this technique, particularly for semiconductor thin-film deposition. Another key point of this study is to investigate the effects of the addition of H_2O on the crystal characteristics and structural properties of ZnO thin films. By providing the fundamental understanding of these processes, this work focuses on laying the foundation for the practical application of ZnO thin films as well as p-n junction/solar cell devices and other electronic applications, ultimately contributing to the advancement of semiconductor thin-film deposition technology using ESD within a very simple framework of fabrication. Further study is required to develop ESD as a novel fabrication process for thin films, which offers high-quality, cost-effective, and very easy to maintain compared to other growth processes and commercial fabrication methods [20]-[26].

This paper follows a structured format. Section 2 provides a concise experimental technique conducted for the work. The results and discussion are presented in Section 3. We conclude and make remarks on this innovative fabrication technique in Section 4.

2. Experimental Procedure

The ESD setup is illustrated in Figures 1(a)-(d). The zinc source used in this study was $ZnCl_2$ (98% Assay $ZnCl_2$). The solutes were CH_3CH_2OH (99.5%, pure) and deionized water (H_2O). ZnO thin films were deposited using the electric field applied spray pyrolysis, named ESD, on the conductive ITiO-coated al-kali-free glass substrates. 20 ml of three different spray solutions were prepared by changing the H_2O ratios. To prepare the first solution with a 0.1 M concentration, 20 ml of CH_3CH_2OH was taken in a glass beaker. The density of CH_3CH_2OH was 0.78945 g/cm^3. Then 0.2726 g $ZnCl_2$ was added with the CH_3CH_2OH in the glass beaker. To make the solution homogeneous, it was heated up to 20 minutes in the magnetic stirrer with a hot plate (ADVANTEC SR/350) (Figure 1(c)). The temperature was considered 150˚C for the magnetic stirrer with a hot plate. Two separate glass beakers were used to prepare the second solution, which consisted of 80% CH_3CH_2OH (16 ml) and 20% H_2O (4 ml), respectively. Next, the same amount of $ZnCl_2$ was added to the glass beaker along with 16 ml of CH_3CH_2OH. The same procedure was applied to prepare the homogeneous spray solution. Then 4 ml of H_2O was poured into the solution containing CH_3CH_2OH and $ZnCl_2$. The mixture of the solution was heated for an additional 10 minutes using a magnetic stirrer with a hot plate. For

the third ESD spray solution, 50% CH_3CH_2OH (10 ml of CH_3CH_2OH) and 50% H_2O (10 ml of H_2O) were taken in two different glass beakers. We followed similar procedures to create a homogenous solution.

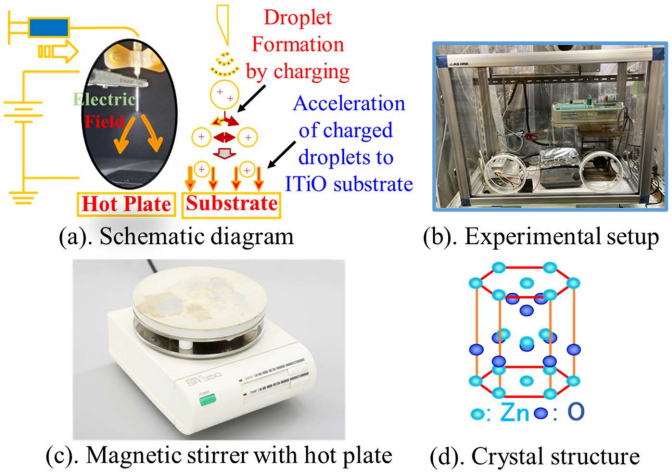

Figure 1. Experimental setup of ESD.

Table 1. Applied ESD parameters for fabrication.

SI. No.	Parameter	Values
1.	Distance between nozzles and the hot plate top	3.5 cm
2.	Flow rate	2.0 ml/h
3.	Deposition time	5 min
4.	Applied voltage	8 kV

The distance between the nozzle and the substrate was 3.5 cm. The precursor solution was pumped through a 0.26 mm diameter metallic nozzle at a flow rate of 2.0 mL/h. The hotplate maintained the surface of the conductive substrate at 300˚C - 500˚C, thereby facilitating the rapid evaporation of the solvent. In this experiment, the main solvent was CH_3CH_2OH, which has a boiling point of 78.37˚C. The conductive substrate was heated on the hot plate for 10 min before the deposition. A voltage of 8 kV was applied between the metallic nozzle and the conductive substrate to form the Taylor cone [27]-[29], after which ESD was carried out for 5 minutes. After the deposition, the sample was kept on the hotplate for 10 minutes to evaporate the solvent thoroughly. For simplification and understanding, the ESD parameters are listed in Table 1 of this investigation. The crystallographic orientations and morphologies of the ZnO films were observed by XRD, SEM, EDX, and Raman, respectively. Furthermore, nanoscale-level studies mainly lattice parameters, a (Å) [30], and c (Å) [20] [30], bond length, (Zn-O bond (Å)) [30] [31], and, positional parameter, μ [30], were investigate to understand the preferential growth of ZnO thin films and how behavior is changing and affected by ESD with changing the H_2O ratios. The average crystallite size, D (Å) was cal-

culated from the XRD peak width of (002) based on the (D-S) method (equation (8)) [25]-[30]. Peak width analysis yields two primary properties, lattice strain ε (%) [20] [32] and dislocation distribution δ (*10^{18} m^2) [32] [33], which have been studied in detail and are correlated to the basic crystal growth mechanism [34] [35]. We will discuss the detailed mathematical formulation of these MIP properties in the next section.

3. Results and Discussion

3.1. Characterization

3.1.1. Structural Analysis

ZnO crystallizes in the wurtzite structure, where oxygen atoms are distributed in a hexagonal close-packed pattern and zinc atoms occupy half of the tetrahedral positions. The Zn and O atoms exhibit tetrahedral coordination with each other, resulting in an identical position. The Zn structure is characterized by an open configuration, where all the octahedral sites and half of the tetrahedral sites are unoccupied. According to Bragg's law [32] [36],

$$n\lambda = 2d\sin\theta \tag{1}$$

where n is the order of diffraction (usually n = 1), λ is the X-ray wavelength and d is the spacing between planes of given Miller indices h, k, and l. In the ZnO hexagonal structure, the plane spacing d is related to the lattice constants a, c, and the Miller indices by the following relation [20] [30],

$$\frac{1}{d_{hkl}^2} = \frac{4}{3}\left(\frac{h^2+k^2+hk}{a^2}\right) + \frac{l^2}{c^2} \tag{2}$$

Considering the first-order approximation, $n = 1$, Equation (2) can be written:

$$\sin^2\theta = \frac{\lambda^2}{4a^2}\left[\frac{4}{3}\left(h^2+k^2+hk\right) + \frac{a^2}{c^2}l^2\right] \tag{3}$$

Following Equation (3), the lattice constant a (Å) for the (100) plane is calculated by [30]

$$a = \frac{\lambda}{\sqrt{3}\sin\theta_{100}} \tag{4}$$

Similarly, for the (002) plane, the lattice constant c (Å) is calculated by Equation (3) [30]

$$c = \frac{\lambda}{\sin\theta_{002}} \tag{5}$$

Moreover, the microstructure parameter, namely bond length (Zn-O) (Å), correlated with the lattice parameter, a, and c is also estimated. The equation used to estimate the bond length for the ZnO thin films is [20] [37]

$$L = \left(\frac{a^2}{3c^2} + \left(0.5-\mu\right)^2 * c^2\right)^{1/2} \tag{6}$$

where (μ) is the positional parameter of the wurtzite structure that indicates the extent of atom displacement relative to the following plane in the c axis, as expressed with Equation (7) [20] [31]

$$\mu = \frac{a^2}{3c^2} + 0.25 \tag{7}$$

The average crystallite size was calculated from the XRD peak width of (002) based on the Debye–Scherrer equation [31]-[43]

$$D = \frac{K\lambda}{\beta \cos\theta} \tag{8}$$

where β is the integral half width, K is a constant equal to 0.90, λ is the wavelength of the incident X-ray (λ = 0.1540 nm), D is the crystallite size, and θ is the Bragg angle.

3.1.2. XRD Analysis

An XRD experiment has been performed to characterize the structural properties of the ZnO thin film growth at 300˚C, 400˚C, and 500˚C temperatures, respectively. **Figures 2(a)-(c)** demonstrate the XRD pattern of the ZnO thin films on conductive ITiO substrate. **Figure 2(a)** represents the XRD results without mixing the H_2O ratio in the spray solution. The data analysis reveals that the fabricated thin film exhibits a hexagonal polycrystalline structure in the wurtzite phase, with the preferential directions being (100), (002), and (101) compared to the JCPDS 36-1451 card for ZnO [44]. Significantly, the (002) plane at 400˚C and 500˚C temperatures exhibits a strong peak at the diffraction angle around 34.50˚C, respectively. At 300˚C temperature, the (100) and (102) planes exhibit very weak peaks compared to 400˚C and 500˚C temperatures. Furthermore, the strong peak for the (100), (002), and (101) planes only appeared at the 500˚C temperature of 0% H_2O ratio. Moreover, the consecutive peak appearance of the (002) plane in the observation corroborated the fabrication of ZnO thin films with a hexagonal wurtzite structure [32]. **Figure 2(b)** illustrates for 20% H_2O ratio, and it shows that there is a strong peak for the (002) plane at 400˚C and 500˚C, respectively. It is also observed that the peak strength for 400˚C temperature is weaker than that of 500˚C temperature. In addition, the peak position (500˚C temperature) shifted slightly to the right, which suggests a decrease in the lattice constant along the c-axis at high temperatures. The peak strength for the (100) plane is found to be weak at temperatures ranging from 400˚C to 500˚C. The other peak positions corresponding to ZnO thin film growth on the ITIO substrates are also observed at the (101) and (102) planes. Interestingly, the peak intensity (102) plane is observed to be stronger compared to **Figure 2(a)**. Gradually, it has become stronger by increasing the H_2O ratio to 50%. This change may be attributed to the transition of the crystal phase from wurtzite to another phase caused by the excessive H_2O ratio. From Raman analysis, it can be correlated that increasing the H_2O ratio suppresses the wurtzite phase, which is elaborately discussed in the corresponding section. **Figure 2(c)** shows the results for a 50% H_2O ratio to ESD spray solution. At 500˚C,

a similar diffraction peak orientation exists for ZnO thin films in the (100), (002), and (102) planes. The (102) plane had a significantly greater peak strength compared to other planes as the temperature increased to 500˚C, as mentioned earlier, due to the H_2O effect. However, the ZnO thin film exhibited a physically significant change at 400˚C in the (100) and (102) planes. The peak intensity on the plane (002) was observed to decrease progressively as the H_2O ratio increased. This complexity may be attributed to the intricate reaction formation that occurs during thin film fabrication using the ESD technique among the $[OH]^-$ and $[Cl]^-$ ionic state reactions, for which we proposed the reaction mechanism in our previous work with the HCl doping effect [23]. We expect that a similar complex reaction mechanism may have occurred in the present study. Moreover, anions might preferentially adsorb onto specific crystal faces and inhibit their growth. At 300˚C, a very small and weak peak could be seen on the crystal planes (100), (002), (101), and (102). Furthermore, a distinct maximum is not observed for the (002) plane in the case of a 50% H_2O ratio. On the other hand, the (002) orientation of the hexagonal wurtzite structure has a small surface energy, which results in a higher growth rate, according to the basic crystal growth theory [37]. But the opposite trend is seen in the higher H_2O ratio than the ESD technique. This trend also explains the possible anisotropy of the fabrication process. The XRD measurements confirm that the deposited thin films exhibit a significant orientation along the c-axis (002), with variations in peak strength almost identical to those reported in the JCPDS 36-1451 card for ZnO [44].

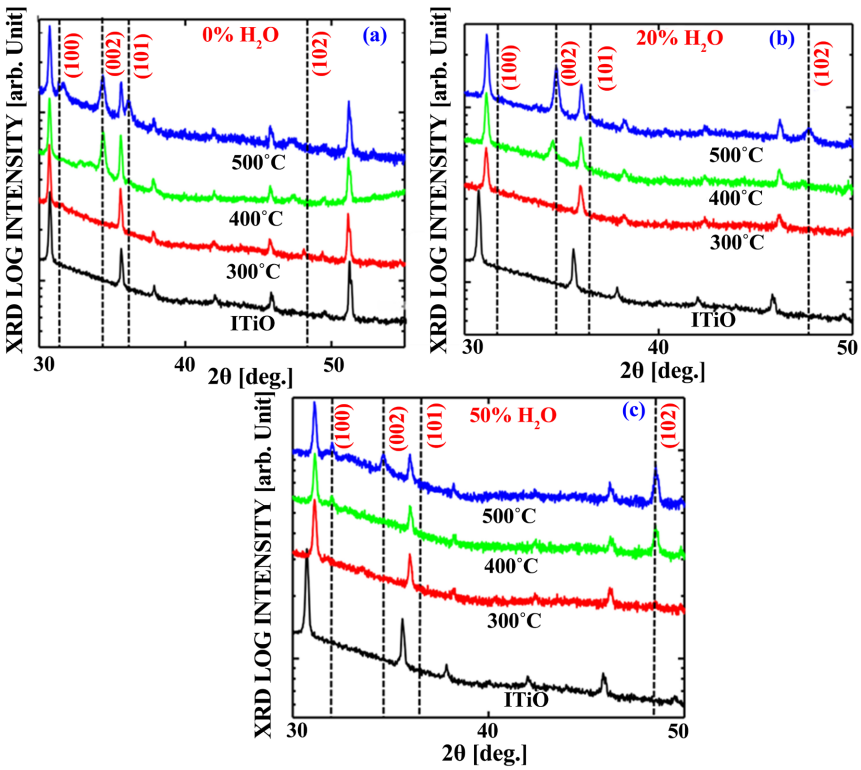

Figure 2. XRD patterns of fabricated ZnO thin film according to the weight ratio of H_2O.

3.1.3. SEM and EDX Analysis

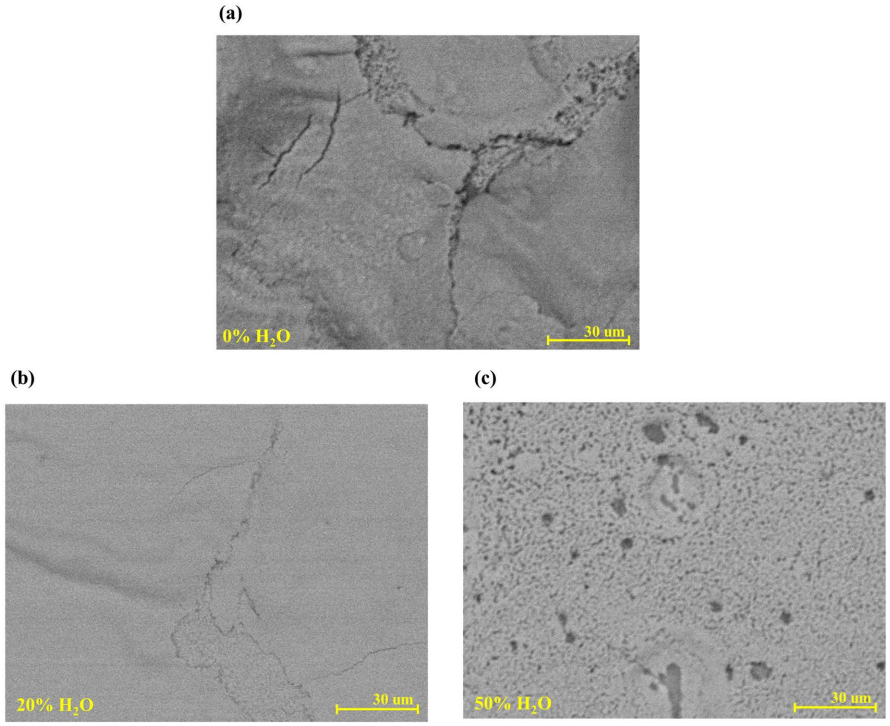

Figure 3. SEM patterns of ZnO thin film according to 0%, 20%, and 50% weight ratio of H_2O in the solution at 500˚C.

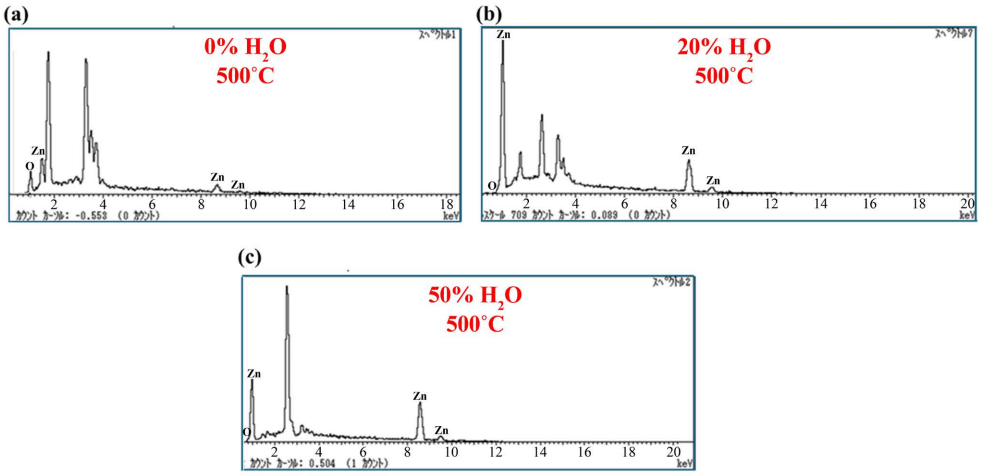

Figure 4. EDX patterns of ZnO film according to 0%, 20%, 50% weight ratio of H_2O in ESD solution at 500˚C.

Next, the surface morphologies of the ZnO thin films were investigated. A representative SEM image of the undoped ZnO thin film is shown in **Figure 3(a)**, revealing that typically 45 - 50 nm grains were grown on the conductive ITIO surface of the ZnO thin film, with each grain being of slightly different size and not agglomerated. Therefore, flat and dense polycrystalline ZnO thin films can be de-

posited by ESD owing to the mono-dispersion, self-dispersion, and non-agglomeration of the charged droplets [20]. The surface morphologies of the H_2O-added ZnO films were slightly different from those without the additive, regardless of the H_2O ratio. However, unidentified particles of a few micrometers were observed only in the ZnO film with 0% H_2O content, as shown in **Figure 3(a)**. These could be unreacted precursors or the zinc oxychloride phase. This result correlated with the change in the composition ratio of H_2O obtained via EDX (**Figure 4**). Additionally, our previous research indicated that oxide thin films fabricated by ESD were extremely flat, boosting an average roughness of approximately 1 nm [19]. Therefore, ESD emerges as a viable deposition method for generating thin films characterized by superior flatness and uniformity, with quality on par with that of dry processes.

3.2. Temperature Effect on Lattice Parameters

The estimated lattice parameters a (Å) and c (Å), using Equations (4) and (5) for this study, are plotted in **Figures 5(a)-(c)** and **Figures 6(a)-(c)**, respectively. It is well known that the lattice parameters are temperature dependent, *i.e.*, an increase in temperature leads to expansion of the lattice [31]. **Figures 5(a)-(c)** showed the changing effect of lattice parameter, a (Å) for the (100) plane, besides **Figures 6(a)-(c)** lattice parameter, c (Å) for the (002) plane; with changing the water ratios and the temperature range from 300˚C to 500˚C. The lattice parameter analysis results showed a very consistent change in behavior. In **Figure 5(a)**, the lattice parameter, a (Å), is slightly decreasing from 300˚C to 400˚C temperature, and then it starts to increase from 400˚C to 500˚C temperature. But, the aptitude of lattice parameter, c (Å), is increasing from 300˚C to 400˚C, and then a very constant increasing behavior is observed from 400˚C to 500˚C in **Figure 6(a)**. **Figure 5(b)** illustrates the result for 20% H_2O mixing in the fabrication process, and the lattice parameter, a (Å), is increasing from 300˚C to 500˚C. But, the tendency of lattice parameter, c (Å), is increasing from 300˚C to 400˚C, and then a decreasing behavior is observed from 400˚C to 500˚C in **Figure 6(b)**. Moreover, the results for a 50% H_2O ratio showed that the lattice parameter, a (Å), is increasing from 300˚C to 400˚C temperature, and then it starts to decrease from 400˚C to 500˚C temperature in **Figure 5(c)**. On the other hand, the lattice parameter, c (Å), is slightly decreasing from 300˚C to 400˚C temperature, and then a very sharp decreasing behavior is found from 400˚C to 500˚C temperature in **Figure 6(c)**. The consistent results can be seen only for the nonmixing of H_2O with the ESD-fabricated thin films. Some experimental results also claim that the possible complex reaction formation may occur due to excessive mixing of H_2O during the fabrication process of ZnO thin film [45]. But the proper reason is not clear yet. Due to this background, further study may be conducted on the different aspects of composition with the H_2O ratio. The lattice parameter ratio, (c/a), is also listed in **Table 2**. Similar results are seen for a (Å), c (Å), and (c/a) to those reported in the (JCPDS 36-1451) card [44].

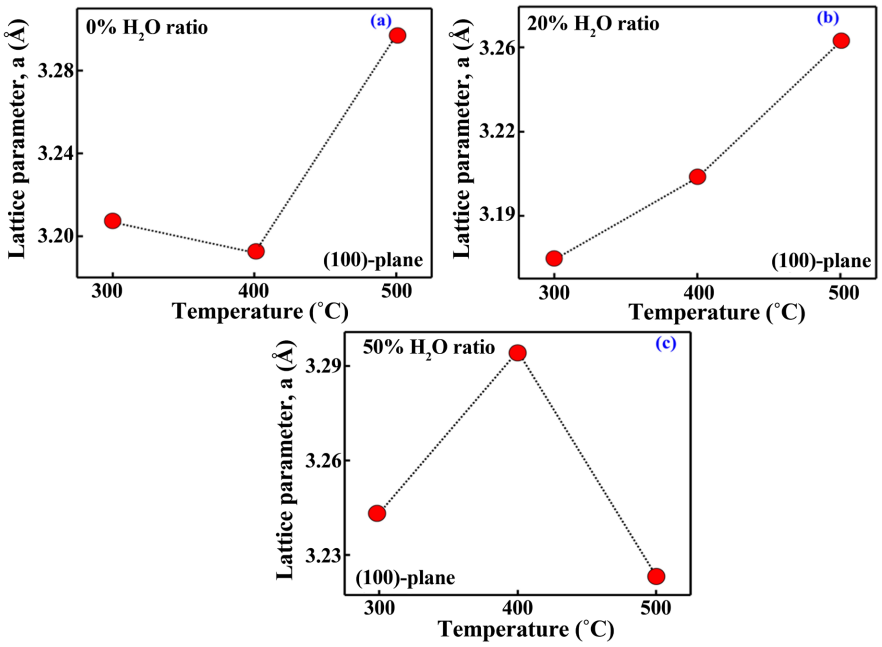

Figure 5. The trend of lattice parameter a (Å) of ZnO film according to the weight ratio of H_2O in the ESD solution at 300˚C, 400˚C, and 500˚C, respectively.

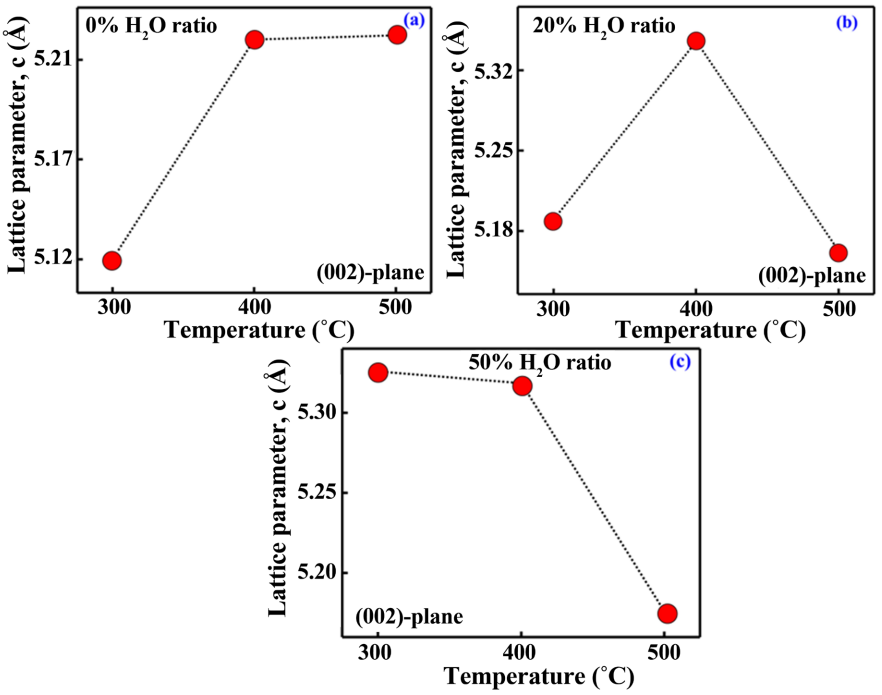

Figure 6. The trend of lattice parameter c (Å) of ZnO film according to the weight ratio of H_2O in the solution deposited by ESD at 300˚C, 400˚C, and 500˚C, respectively.

3.3. Temperature Effect on Lattice Bond Length

The detailed estimated results of the positional parameter μ are listed in Table 2. A random changing trend is observed for μ with the H_2O ratio. So, accurate pre-

diction related to the atomic displacement and the structural correlation may be difficult at this point. In Figure 7(a), for the 0% H_2O ratio ESD sample, the nature of bond length, (Zn-O) (Å), shows a very small decrease from 300˚C to 400˚C temperature, and then it starts to increase from 400˚C to 500˚C temperature. On the other hand, Figure 7(b) illustrates the results for a 20% H_2O ratio and an increase from 300˚C to 400˚C temperature, then a very constant nature was observed from 400˚C to 500˚C temperature. This is correlated to the decreasing lattice constant parameter, c (Å), in this temperature range. The results for the 50% H_2O ratio showed the decreasing nature from 400˚C to 500˚C temperature (Figure 7(c)). This is due to both the lattice constant parameter, a (Å), and c (Å) being found to decrease in nature except for the 300˚C to 400˚C temperature range of lattice constant parameter, a (Å). The results obtained for ZnO bond length (Zn-O) (Å) for this study are found to be in good agreement with the 1.98 (Å) reported in the literature [31] [32].

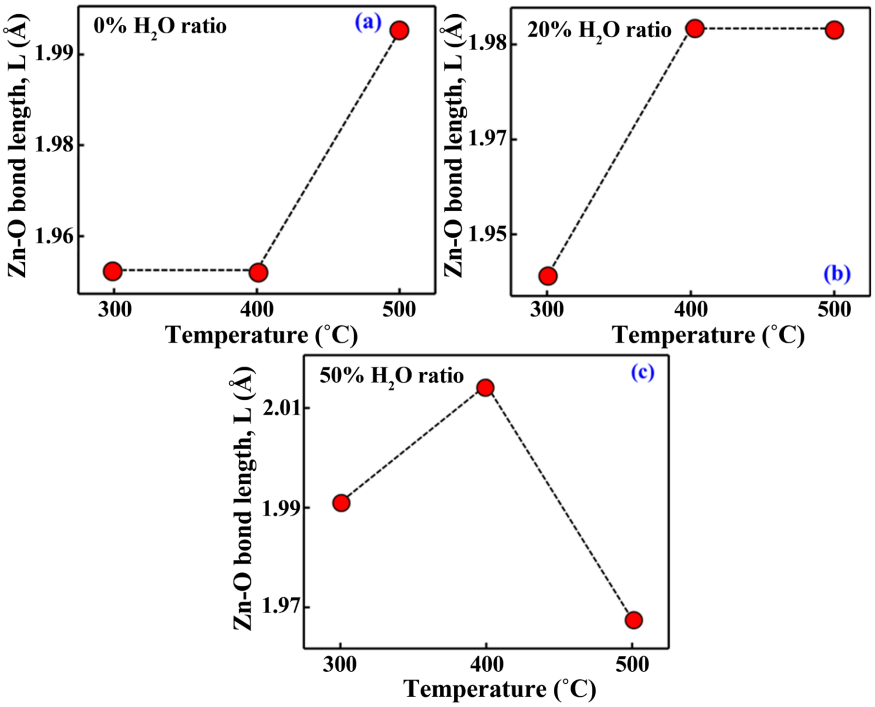

Figure 7. Changing phenomena of bond length L (Å) of ZnO thin film according to the weight ratio of H_2O at different temperatures.

3.4. Temperature Effect on Crystallite

It is known that a perfect crystal would ideally continue infinitely in all directions, but in reality, all crystals are imperfect since they have a limited size [32]. The broadening of diffraction peaks in materials occurs due to the deviation from perfect crystallinity. Crystallite size, D (Å), refers to the dimensions of a domain that exhibits coherent diffraction. It is important to note that the crystallite size of particles is typically different from their particle size because of the existence of polycrystalline aggregates. Lattice strain ε (%) is a measure of the distribution of lat-

tice constants (a (Å), and c (Å)) arising from crystal imperfections, such as lattice dislocation, δ (*10^{16} m^2). The X-ray line broadening is used for the investigation of dislocation distribution, δ (*10^{16} m^2). In the present study, it was found that the ZnO (002) plane diffraction peak is much stronger than the ZnO (101) peak (Figures 2(a)-(c)). This indicates that the formation of ZnO nanocrystals has a preferential crystallographic (002) orientation. The average crystallite size calculated for synthesized ZnO nanoparticles was 47.77 nm by the ESD technique.

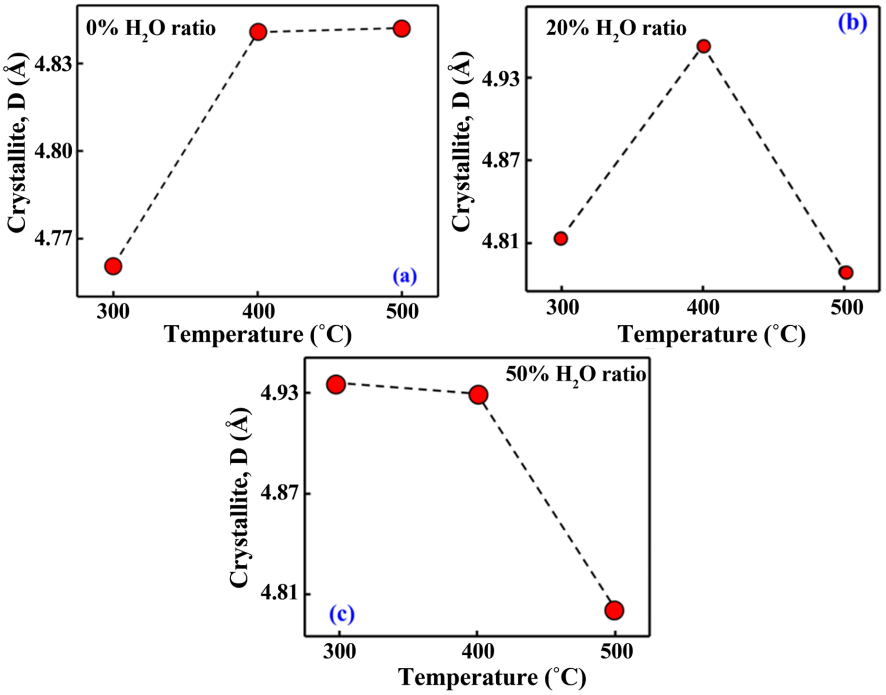

Figure 8. The trend of (a-c) lattice crystallite D (Å) of ZnO thin film according to the weight ratio of H_2O at different temperatures.

Table 2. Microstructural parameters with changing H_2O ratio.

H_2O Ratio	Temperature (˚C)	Lattice Constant Ratio [(c/a)]	Positional Parameter (μ)	FWHM	Dislocation Density (d*10^{16}) [m^{-2}]	Lattice Strain (ε) %
0%	300	1.598	0.381	0.0413	4.412	0.242
	400	1.634	0.374	0.2707	4.271	0.243
	500	1.583	0.383	0.3382	4.264	0.242
20%	300	1.634	0.375	0.0263	4.307	0.242
	400	1.667	0.370	0.329	4.077	0.243
	500	1.585	0.383	0.2468	4.351	0.242
50%	300	1.64	0.374	0.1323	4.105	0.243
	400	1.612	0.378	0.0511	4.115	0.243
	500	1.604	0.381	0.2351	4.330	0.242

The crystallite size is assumed to be the size of a coherently diffracting domain, and it is not necessarily the same as particle size. The measured crystallite size D (Å) (**Figures 8(a)-(c)**) of the films is observed to exhibit similar behavior compared to the lattice constant parameter c (Å) (**Figures 6(a)-(c)**), temperature 300˚C to 500˚C. This behavior is consistent and supports the growth mechanism of ZnO thin film [32] [37] by the ESD technique. The dislocation density (δ), and lattice strain (ε), FWHM of the deposited ZnO thin films are listed in **Table 2**. It should be noted that a higher dislocation density (δ) is always significantly important for the fabrication of high-quality crystal-thin films [31]. In the present study, the route of thin film fabrication by ESD has proven the potential impact for thin film fabrication, and in the future, this device fabrication could also be implemented for solar cells and other optoelectronic device applications for technological advancement. Besides tuning the ESD parameters, the dislocation density (δ) could also be tuned which is another potential impact for easy device usage.

3.5. Raman Spectroscopy

Raman spectroscopy can provide insights into several complex molecular phenomena in a substance, including the identification of multiple phases within the same material. Moreover, it facilitated the examination of transitions from amorphous to crystalline phases, diverse flaws, and stress conditions. The current experiment demonstrated the development of thin ZnO films with a hexagonal wurtzite structure. The literature [38] states that ZnO is a semiconductor material with has c_{6v}^4 spatial symmetry. Group theory states that there are $A_1 + 2E_2 + E_1$ modes that are related to ZnO, which has a total of four atoms in each unit cell for its hexagonal wurtzite structure [35]. This arrangement results in 12 phonon branches, with nine being optical modes and three being acoustic modes. **Figure 9** shows the Raman spectrum of the ZnO thin film for 500˚C temperature of exchanging H_2O ratio. The Raman peaks around 475 cm^{-1} and 780 cm^{-1} were assigned to ZnO E_2 (high) and A_1 longitudinal optical (LO) modes, respectively, for 0% H_2O. Furthermore, other multiphonon modes were also observed, such as transverse phonon (TA), low-order phonon (E_1), mixed phonon (TA + LA), and second-order phonon for longitudinal phonon (A_2). This phenomenon decreases as the H_2O ratio increases to 20% and 50%. Only the effective Raman phenomena are observed for the 0% H_2O ratio. Raman spectroscopy of the E_2 phonons plays a significant role in the study of residual stress in ZnO thin film crystals; that residual stress correlates with the complex growth mechanism in wurtzite structure crystals [45]. This study observes that the E_2 phonon mode gradually decreases as the H_2O ratios increase [37] (**Figures 9(a)-(c)**). A decrease in the E_2 phonon frequency is attributed to tensile stress, while its increase is attributed to compressive stress. The study under this investigation, the E_2 vibration mode at 475 cm^{-1} is characteristic of the wurtzite phase, and its value is higher than 439 cm^{-1} for the tensile stress-free bulk ZnO thin film [35], suggesting that the fabricated ZnO thin films are exhibiting low tensile stress for the 0% H_2O. On the other hand, 20% and

50% H_2O ratio mixing fabricated ZnO thin film possesses very high tensile stress. Due to this high tensile stress, the corresponding Raman peaks are found to be very weak and have disappeared, respectively. This analysis provides us with two possibilities. First, the tensile stress probably originated from a mismatch in the thermal expansion coefficient of the ZnO thin film (4.75×10^{-6} K^{-1}) and the glass substrate (2.60×10^{-6} K^{-1}). This mismatch may correlate with crystal defects and anisotropy of the thin films [40]. Second, the possible existence of complex reaction formation due to excessive H_2O carried to the excessive amount of the leaving group $[OH]^-$ compound. As a result, the kinetics of ZnO nanoparticles or/ dipole moment changing tendency may occur in the fabrication process [38]. Moreover, the A_1 (LO) mode at 780 cm^{-1} originates from defects such as oxygen vacancies and Zn interstitials [39], and its relatively low intensity peak indicates a relatively low density of defects in the ZnO thin films. This corroborates the experimental XRD analysis by the ESD technique (**Figures 2(a)-(c)**). The weak peak at 260 cm^{-1} was attributed to the second-order Raman processes for 0% H_2O ratio. In addition, the second-order Raman modes are increased with increasing the H_2O ratios. Further study is required to understand this lattice anisotropy and the complex reaction mechanism of ESD with different solution formats.

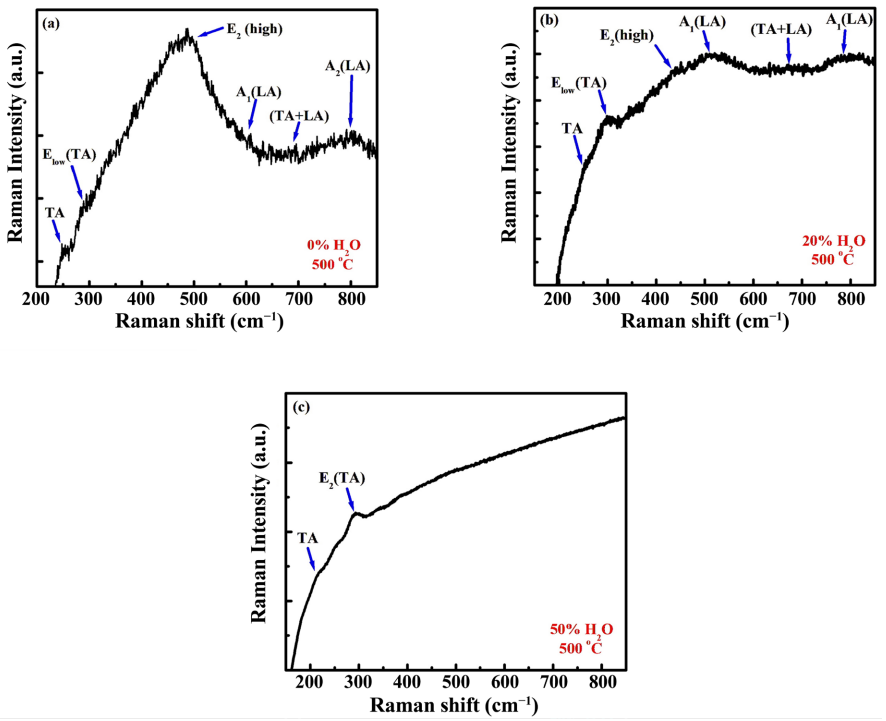

Figure 9. Raman spectra of the ZnO thin films of $ZnCl_2$ and CH_3CH_2OH precursor solution by ESD at 500˚C temperature, ESD sample with micro-ring structures.

4. Conclusions

The ESD approach for the next generation of ZnO thin films on conductive ITIO

substrates, along with the solution dependency analysis of these studies, led us to make the following concluding remarks.

(i) ESD is a highly effective technique for the fabrication of high-quality ZnO thin films, demonstrating substantial advantages over conventional deposition methods. Unlike conventional methods, ESD utilizes charged droplets to achieve precise control over film uniformity and density, resulting in superior film quality with excellent surface flatness and uniformity, as well as fewer defects and reduced material wastage.

(ii) XRD analysis revealed that the doping of the H_2O ratio to the ESD solution significantly affected the crystallite of the lattice, while SEM and EDX verified the effect of ZnO in the films. The XRD results also demonstrate the growth of ZnO thin films with a hexagonal wurtzite structure. In addition, the preferred crystal orientation for the (002) plane is very effective at 500˚C for 0% H_2O and 20% H_2O ratio, whereas a 50% H_2O ratio showed a possible change of crystal phase.

(iii) The MIP properties such as lattice parameters a (Å), c (Å), their ratio, lattice crystallite, bond length (Zn-O bond) (Å), μ, ε (%), and δ ($*10^{18}$ m^2) were found in the same order of range compared to other fabrication processes of ZnO thin film.

(iv) The decreasing tendency of Raman peaks and the increasing tendency of the second-order phonon mode are observed with increasing H_2O ratios. It indicates that the possible excess enthalpy stored in nanocrystalline materials originates from the distorted crystallites. Further studies are required to reveal these phenomena related to thin film growth.

(v) Finally, XRD, SEM, and Raman studies show that $ZnCl_2$ and the CH_3CH_2OH precursor solution, when combined with the ESD fabrication technique, can significantly contribute to the formation of high-quality thin films with the suitable doping of the H_2O ratio.

These findings highlight the capability of ESD to enhance semiconductor thin-film technology, facilitating more economical and scalable production techniques.

Acknowledgements

The authors express their sincere appreciation to ESD research group members at Sugiyama Laboratory at Tokyo University of Science for their support in completing the experiments and for the constructive discussions.

Authors' Contributions

F.I.A.: Conceptualization, investigation, writing-original draft, plotting figures, methodology, software, review & editing; M.S.: Supervising, writing-original draft, review & editing.

Data Availability

The raw/processed data required to reproduce these findings can be shared upon request.

Conflicts of Interest

The authors declare no conflicts of interest regarding the publication of this paper.

References

[1] Hibino, K., Olejníček, J., Yamanoi, K., Ponseca, C.S., Shuaib, A., Maruyama, Y., *et al.* (2025) Impact of Electron Cyclotron Wave Resonance Plasma on Defect Reduction in ZnO Thin Films. *Scientific Reports*, **15**, Article No. 5555. https://doi.org/10.1038/s41598-025-88921-5

[2] Choi, Y., Kang, J., Hwang, D. and Park, S. (2010) Recent Advances in ZnO-Based Light-Emitting Diodes. *IEEE Transactions on Electron Devices*, **57**, 26-41. https://doi.org/10.1109/ted.2009.2033769

[3] Baruah, S. and Dutta, J. (2009) Hydrothermal Growth of ZnO Nanostructures. *Science and Technology of Advanced Materials*, **10**, Article 013001. https://doi.org/10.1088/1468-6996/10/1/013001

[4] Dolabella, S., Borzì, A., Dommann, A. and Neels, A. (2022) Lattice Strain and Defects Analysis in Nanostructured Semiconductor Materials and Devices by High-Resolution X-Ray Diffraction: Theoretical and Practical Aspects. *Small Methods*, **6**, Article 2100932. https://doi.org/10.1002/smtd.202100932

[5] Zhu, L. and Zeng, W. (2017) Room-Temperature Gas Sensing of ZnO-Based Gas Sensor: A Review. *Sensors and Actuators A*: *Physical*, **267**, 242-261. https://doi.org/10.1016/j.sna.2017.10.021

[6] Srikanth, C.K. and Jeevanandam, P. (2009) Effect of Anion on the Homogeneous Precipitation of Precursors and Their Thermal Decomposition to Zinc Oxide. *Journal of Alloys and Compounds*, **486**, 677-684. https://doi.org/10.1016/j.jallcom.2009.07.031

[7] Chu, S., Olmedo, M., Yang, Z., Kong, J. and Liu, J. (2008) Electrically Pumped Ultraviolet ZnO Diode Lasers on Si. *Applied Physics Letters*, **93**, Article 181106. https://doi.org/10.1063/1.3012579

[8] Ram, S.D.G., Kulandainathan, M.A. and Ravi, G. (2010) Aqueous Chemical Growth of Free Standing Vertical ZnO Nano Prisms, Nanorods and Nano Diskettes with Improved Texture Co-Efficient and Tunable Size Uniformity. *Applied Physics A*, **105**, 881-890.

[9] Park, J.B., Song, M.S., Ghosh, R., Saroj, R.K., Hwang, Y., Tchoe, Y., *et al.* (2021) Highly Sensitive and Flexible Pressure Sensors Using Position- and Dimension-Controlled ZnO Nanotube Arrays Grown on Graphene Films. *NPG Asia Materials*, **13**, Article No. 57. https://doi.org/10.1038/s41427-021-00324-w

[10] Thomas, D.G. (1960) The Exciton Spectrum of Zinc Oxide. *Journal of Physics and Chemistry of Solids*, **15**, 86-96. https://doi.org/10.1016/0022-3697(60)90104-9

[11] Otieno, F., Airo, M., Erasmus, R.M., Quandt, A., Billing, D.G. and Wamwangi, D. (2020) Annealing Effect on the Structural and Optical Behavior of ZnO: Eu3+ Thin Film Grown Using RF Magnetron Sputtering Technique and Application to Dye Sensitized Solar Cells. *Scientific Reports*, **10**, Article No. 8557. https://doi.org/10.1038/s41598-020-65231-6

[12] Dutta, T., Gupta, P., Gupta, A. and Narayan, J. (2010) Effect of Li Doping in Nio Thin Films on Its Transparent and Conducting Properties and Its Application in Heteroepitaxial P-N Junctions. *Journal of Applied Physics*, **108**, Article 083715. https://doi.org/10.1063/1.349927

[13] Xia, X.H., Tu, J.P., Zhang, J., Wang, X.L., Zhang, W.K. and Huang, H. (2008) Morphology Effect on the Electrochromic and Electrochemical Performances of NiO Thin Films. *Electrochimica Acta*, **53**, 5721-5724. https://doi.org/10.1016/j.electacta.2008.03.047

[14] Justh, N., Bakos, L.P., Hernádi, K., Kiss, G., Réti, B., Erdélyi, Z., *et al.* (2017) Photocatalytic Hollow TiO_2 and ZnO Nanospheres Prepared by Atomic Layer Deposition. *Scientific Reports*, **7**, Article No. 4337. https://doi.org/10.1038/s41598-017-04090-0

[15] Reguig, B.A., Khelil, A., Cattin, L., Morsli, M. and Bernède, J.C. (2007) Properties of Nio Thin Films Deposited by Intermittent Spray Pyrolysis Process. *Applied Surface Science*, **253**, 4330-4334. https://doi.org/10.1016/j.apsusc.2006.09.046

[16] Tijani, N.A., Akintayo, O.A., Animasahun, L.O., Ajani, T.F., Ungokore, H.Y., Maphiri, V.M., *et al.* (2024) Preparation, Characterization and Biological Activity of Co-Doped ZnO Nanostructured Thin Film: A Comprehensive Study on Its Photo-Physical Properties and Antimicrobial Efficacy against Food-Borne Pathogen. *Optical Materials*, **157**, Article 116325. https://doi.org/10.1016/j.optmat.2024.116325

[17] Atta, D., Wahab, H.A., Ibrahim, M.A. and Battisha, I.K. (2024) Photocatalytic Degradation of Methylene Blue Dye by ZnO Nanoparticle Thin Films, Using Sol-Gel Technique and UV Laser Irradiation. *Scientific Reports*, **14**, Article No. 26961. https://doi.org/10.1038/s41598-024-76938-1

[18] Smajlagić, A., Modrić-Šahbazović, A., Sakić, Z. and Babajić, E. (2024) Synthesis, Characterization and Optical Morphology of ZnO Nanoparticles. *Open Journal of Applied Sciences*, **14**, 1330-1337. https://doi.org/10.4236/ojapps.2024.145087

[19] Tomono, K. and Sugiyama, M. (2024) Investigating Electrical Properties and Crystal Growth in Nio Thin Films by Spray Pyrolysis and Electrostatic Spray Deposition. *Japanese Journal of Applied Physics*, **63**, Article 025504. https://doi.org/10.35848/1347-4065/ad1f09

[20] Okubo, K. and Sugiyama, M. (2024) Effects of Li Concentration in the Precursor Solution on Nio Thin Films Deposited Using Electrostatic Spray Deposition. *Japanese Journal of Applied Physics*, **63**, Article 111006. https://doi.org/10.35848/1347-4065/ad8c07

[21] Abbas, F.I. and Sugiyama, M. (2024) Solution-Dependent Electrostatic Spray Deposition (ESD) ZnO Thin Film Growth Processes.

[22] Abbas, F.I. and Sugiyama, M. (2024) Investigation the Anisotropic Feature Using Structural and Mechanical Profile Analysis of Zinc Oxide (ZnO) Thin Film Growth Mechanism within the Framework of Williamson-Hall Estimation by Novel Electrostatic Spray Deposition (ESD) Technique. *Journal of Physics: Applications and Mechanics*, **1**, 1-9. https://doi.org/10.47739/physics.1005

[23] Abbas, F.I. and Sugiyama, M. (2025) Novel Electrostatic Spray Deposition (ESD) Techniques for Growth Mechanisms of Solution-Dependent Zinc Oxide (ZnO) Thin Films. *Journal of Applied Material Science & Engineering Research*, **9**, 1-9. https://doi.org/10.33140/jamser.09.01.03

[24] Abbas, F.I. and Sugiyama, M. (2025) A Comparative Study of Property Measurement for ZnO-Thin Film Growth Processes Using Hydrocloric Acid (HCL) and Water (H_2O) Solution-Dependent on Novel Electrostatic Spray Deposition (ESD). *Latvian Journal of Physics and Technical Sciences*, **62**, 30-41. https://doi.org/10.2478/lpts-2025-0011

[25] Abbas, F.I. and Sugiyama, M. (2025) Anisotropic Role on Zinc Oxide (ZnO) Thin Film Growth Processes of Solution-Dependent Novel Electrostatic Spray Deposition (ESD). *European Journal of Engineering and Technology Research*, **10**, 1-8. https://doi.org/10.24018/ejeng.2025.10.2.3227

[26] Abbas, F.I. and Sugiyama, M. (2025) ZnO-Thin Film Growth Processes: Correlation between the Structural Properties of Hydrochloric Acid (HCL) and Water (H_2O) Solution Effect Using Innovative Electrostatic Spray Deposition (ESD) Technology. *Latvian Journal of Physics and Technical Sciences*, **62**, 68-76. https://doi.org/10.2478/lpts-2025-0023

[27] Joffre, G., Prunet-Foch, B., Berthomme, S. and Cloupeau, M. (1982) Deformation of Liquid Menisci under the Action of an Electric Field. *Journal of Electrostatics*, **13**, 151-165. https://doi.org/10.1016/0304-3886(82)90005-5

[28] Joffre, G.-H. and Cloupeau, M. (1986) Characteristic Forms of Electrified Menisci Emitting Charges. *Journal of Electrostatics*, **18**, 147-161. https://doi.org/10.1016/0304-3886(86)90002-1

[29] Cloupeau, M. and Prunet-Foch, B. (1989) Electrostatic Spraying of Liquids in Cone-Jet Mode. *Journal of Electrostatics*, **22**, 135-159. https://doi.org/10.1016/0304-3886(89)90081-8

[30] Bindu, P. and Thomas, S. (2014) Estimation of Lattice Strain in ZnO Nanoparticles: X-Ray Peak Profile Analysis. *Journal of Theoretical and Applied Physics*, **8**, 123-134. https://doi.org/10.1007/s40094-014-0141-9

[31] Cullity, B.D. (1956) Element of X-Ray Diffraction. Prentice Hall.

[32] Kumar, V., Sharma, H., Singh, S.K., Kumar, S. and Vij, A. (2019) Enhanced Near-Band Edge Emission in Pulsed Laser Deposited ZnO/C-Sapphire Nanocrystalline Thin Films. *Applied Physics A*, **125**, Article No. 212. https://doi.org/10.1007/s00339-019-2485-0

[33] Pal, U., Serrano, J.G., Santiago, P., Xiong, G., Ucer, K.B. and Williams, R.T. (2006) Synthesis and Optical Properties of ZnO Nanostructures with Different Morphologies. *Optical Materials*, **29**, 65-69. https://doi.org/10.1016/j.optmat.2006.03.015

[34] Saleem, M., Fang, L., Ruan, H.B, Wu, F., Huang, Q.L., Xu, C.L. and Kong, C.Y. (2012) Effect of Zinc Acetate Concentration on the Structural and Optical Properties of ZnO Thin Films Deposited by Sol-Gel Method. *International Journal of Physical Sciences*, **7**, 2971-2979.

[35] Singh, S.K. and Singhal, R. (2018) Thermal-Induced SPR Tuning of Ag-ZnO Nanocomposite Thin Film for Plasmonic Applications. *Applied Surface Science*, **439**, 919-926. https://doi.org/10.1016/j.apsusc.2018.01.112

[36] Pope, C.G. (1997) X-Ray Diffraction and the Bragg Equation. *Journal of Chemical Education*, **74**, 129-131. https://doi.org/10.1021/ed074p129

[37] Raoufi, D. (2013) Synthesis and Microstructural Properties of ZnO Nanoparticles Prepared by Precipitation Method. *Renewable Energy*, **50**, 932-937. https://doi.org/10.1016/j.renene.2012.08.076

[38] Huang, Y., Liu, M., Li, Z., Zeng, Y. and Liu, S. (2003) Raman Spectroscopy Study of ZnO-Based Ceramic Films Fabricated by Novel Sol-Gel Process. *Materials Science and Engineering*: *B*, **97**, 111-116. https://doi.org/10.1016/s0921-5107(02)00396-3

[39] Yahia, S.B., Znaidi, L., Kanaev, A. and Petitet, J.P. (2008) Raman Study of Oriented ZnO Thin Films Deposited by Sol-Gel Method. *Spectrochimica Acta Part A*: *Molecular and Biomolecular Spectroscopy*, **71**, 1234-1238. https://doi.org/10.1016/j.saa.2008.03.032

[40] Alim, K.A., Fonoberov, V.A. and Balandin, A.A. (2005) Origin of the Optical Phonon Frequency Shifts in ZnO Quantum Dots. *Applied Physics Letters*, **86**, Article 053103. https://doi.org/10.1063/1.1861509

[41] Wang, L., Pu, Y., Chen, Y.F., Mo, C.L., Fang, W.Q., Xiong, C.B., *et al.* (2005) MOCVD Growth of ZnO Films on Si (111) Substrate Using a Thin AlN Buffer Layer. *Journal of Crystal Growth*, **284**, 459-463. https://doi.org/10.1016/j.jcrysgro.2005.06.058

[42] Lu, K. and Sun, N.X. (1997) Grain-Boundary Enthalpy of Nanocrystalline Selenium. *Philosophical Magazine Letters*, **75**, 389-395. https://doi.org/10.1080/095008397179462

[43] Chatterjee, P.P., Pabi, S.K. and Manna, I. (1999) An Allotropic Transformation Induced by Mechanical Alloying. *Journal of Applied Physics*, **86**, 5912-5914. https://doi.org/10.1063/1.371612

[44] Chung, F.H. (1974) Quantitative Interpretation of X-Ray Diffraction Patterns of Mixtures. I. Matrix-Flushing Method for Quantitative Multicomponent Analysis. *Journal of Applied Crystallography*, **7**, 519-525. https://doi.org/10.1107/s0021889874010375

[45] Vega-Poot, A.G., Rodríguez-Gattorno, G., Soberanis-Domínguez, O.E., Patiño-Díaz, R.T., Espinosa-Pesqueira, M. and Oskam, G. (2010) The Nucleation Kinetics of ZnO Nanoparticles from $ZnCl_2$ in Ethanol Solutions. *Nanoscale*, **2**, Article 2710. https://doi.org/10.1039/c0nr00439a